1986

Asymmetry measurement of the 2s1/2(hy1s1/2 relativistic magnetic-dipole matrix element in He+

A. Van Wijngaarden

J. Patel

Gordon W. F. Drake
University of Windsor

Asymmetry measurement of the $2s_{1/2}$-$1s_{1/2}$ relativistic magnetic-dipole matrix element in He^+

A. van Wijngaarden, J. Patel, and G. W. F. Drake
Department of Physics, University of Windsor, Windsor, Ontario, Canada N9B 3P4
(Received 26 August 1985)

When a beam of spin-polarized $He^+(2s_{1/2})$ ions is quenched by an electric field **E**, the emitted radiation intensity contains a left-right-asymmetry term proportional to $\mathbf{P}\cdot\hat{\mathbf{k}}\times\hat{\mathbf{E}}$, where **P** is the spin-polarization vector and $\hat{\mathbf{k}}$ is the observation direction. The resulting asymmetry is proportional to the relativistic magnetic dipole matrix element $\langle 1s_{1/2,1/2}|M_{1,0}|2s_{1/2,1/2}\rangle$. The measured asymmetry $(2.935\pm0.337)\times10^{-4}$ corresponds to the matrix element $\langle 1s_{1/2,1/2}|M_{1,0}|2s_{1/2,1/2}\rangle = -(0.2725\pm0.0313)\alpha^2 e\hbar/mc$, in agreement with the theoretical value $-0.2794\alpha^2 e\hbar/mc$. The measurement provides a direct test of the relativistic corrections to the magnetic dipole transition operator.

I. INTRODUCTION

The metastable $2^2S_{1/2}$ state in hydrogenic systems can decay to the $1^2S_{1/2}$ ground state by $2E1$ radiation[1,2] and also by $M1$ radiation[2,3] with the emission of a single photon. The former scales as Z^6, while the $M1$ decay rate scales as Z^{10} and becomes the dominant decay mechanism for hydrogenic ions with $Z>43$. Although no precise measurements for the magnetic dipole ($M1$) decay rate exist, its effects have recently been clearly identified. Thus the measured total decay rate of hydrogenic Ar by Gould and Marrus[4] is in agreement with theory only when the 3.2% contribution of $M1$ is taken into account. When we regard their measurement as a measurement of the $M1$ decay rate, assuming that theory for the dominant $2E1$ decay is accurate, then it yields a matrix element at the $\pm32\%$ precision level.

In an earlier paper[5] we demonstrated a technique for directly measuring the magnetic dipole matrix element ($\overline{M}=\langle 1s_{1/2,1/2}|M_{1,0}|2s_{1/2,1/2}\rangle$) by exploiting the interference effects between the Stark-induced $E1$ quench radiation of the $2s_{1/2}$ state and the spontaneous magnetic dipole radiation. By repeated measurements, rejecting values that were more than two standard deviations from the average, we obtained a measurement of $\overline{M}$ for the decay of the $2s_{1/2}$ state in He^+ at the 30% precision level. This paper describes a new measurement in the 10% precision range with much improved apparatus. The measurement is of fundamental importance because the effect vanishes in the absence of relativistic corrections to the magnetic dipole transition operator. It, therefore, provides a direct check of the relativistic corrections in a hydrogenic ion where the matrix elements can be calculated exactly.

In the next section, the theoretical results for the angular distribution of Lyman-α quench radiation is briefly summarized. Sec. III deals with experimental details, followed by Secs. IV and V presenting results and discussion.

II. THEORY

A. Basic formalism

The angular distributions in the electric field quenching radiation[5] when observed with photon polarization insensitive detectors only depends upon the relative orientations of the three vectors **k**, **P**, and **E**. Here **k** is the photon wave vector ($|\mathbf{k}|=\omega/c$), **P** is the electron spin-polarization vector of the ion beam ($|\mathbf{P}|\le1$), and **E** is the electric field vector. The emitted intensity per unit solid angle in an arbitrary observation direction $\hat{\mathbf{k}}$ is then

$$I(\hat{\mathbf{k}})=\frac{\alpha k}{2\pi}[J_0(\hat{\mathbf{k}})-3\,\mathrm{Im}(V_{1/2}^{*}V_{3/2})(\hat{\mathbf{k}}\cdot\hat{\mathbf{E}})(\mathbf{P}\cdot\hat{\mathbf{k}}\times\hat{\mathbf{E}}) + \overline{M}\,\mathrm{Re}(2V_{1/2}+V_{3/2})(\mathbf{P}\cdot\hat{\mathbf{k}}\times\hat{\mathbf{E}}) + 2\overline{M}\,\mathrm{Im}(V_{1/2}-V_{3/2})\hat{\mathbf{k}}\cdot\hat{\mathbf{E}}]\,, \tag{2.1}$$

where

$$J_0(\hat{\mathbf{k}})=\tfrac{1}{2}|V_{1/2}+2V_{3/2}|^2[1-(\hat{\mathbf{k}}\cdot\hat{\mathbf{E}})^2] + \tfrac{1}{2}|V_{1/2}-V_{3/2}|^2[1+(\hat{\mathbf{k}}\cdot\hat{\mathbf{E}})^2]+\overline{M}^2\,, \tag{2.2}$$

$$V_J=\frac{e^2|\mathbf{E}|}{3}\frac{\langle 1s|z|2p\rangle\langle 2p|z|2s\rangle}{E(2s_{1/2})-E(2p_j)+i\Gamma/2},\quad j=\tfrac{1}{2},\tfrac{3}{2} \tag{2.3}$$

in the limit of weak fields where first-order perturbation theory holds.

$$\overline{M}=\langle 1s_{1/2,1/2}|M_{1,0}|2s_{1/2,1/2}\rangle$$

is the matrix element of the relativistic magnetic dipole operator[3]

$$M_{1,0}=\mu_z\left[1-\frac{2p^2}{3mc^2}-\frac{1}{6}\left[\frac{\omega r}{c}\right]^2+\frac{Ze^2}{3mc^2r}\right]. \tag{2.4}$$

Equations (2.1) and (2.2) do not include the negligibly small contributions from magnetic quadrupole transitions via the $2p_{3/2}$ state or other relativistic corrections of order $(\alpha Z)^2$.

The terms in (2.1) are written in order of decreasing magnitude. The first two terms in (2.2) are the dominant electric field quenching terms, while the last one gives a negligibly small contribution from spontaneous magnetic dipole radiation to the ground state. The present experiment is designed to measure the third term in (2.1), which is the interference term between spontaneous magnetic dipole radiation and the electric field induced quench radiation. When the photons are observed perpendicular to the electric field direction ($\hat{\mathbf{k}}\cdot\hat{\mathbf{E}}=0$), (2.1) simplifies to

$$I(\hat{\mathbf{k}})=\frac{\alpha k}{2\pi}[J_0(\hat{\mathbf{k}})+\overline{M}\,\mathrm{Re}(2V_{1/2}+V_{3/2})(\mathbf{P}\cdot\hat{\mathbf{k}}\times\hat{\mathbf{E}})] \ . \tag{2.5}$$

As can be seen from (2.1), this equation is also approximately valid for the radiation emitted over a small angular range along the field where $\hat{\mathbf{k}}\times\hat{\mathbf{E}}\rightarrow 0$.

B. Angular distribution

The geometry of the experiment is such that **P** and **E** are orthogonal and $\hat{\mathbf{k}}$ lies in the plane perpendicular to the beam axis as shown in Fig. 1. When θ is the angle between $\hat{\mathbf{k}}$ and **E** and the intensity in the $\theta=\pi/2$ direction is normalized to unity, then the J_0 term (at small electric fields) has the distribution

$$\mathscr{L}(\theta)=1+0.2675\cos^2\theta \ , \tag{2.6}$$

and as shown in Sec. II C the angular distribution of the second term in (2.5) (the magnetic dipole interference term) has the distribution

$$\mathscr{M}(\theta)=\pm|\mathbf{P}|\left[\frac{0.013\,13}{|\mathbf{E}|}\right]\left[1-\frac{0.013\,13}{|\mathbf{E}|}\right]^{-1}\sin\theta \ . \tag{2.7}$$

The + sign applies when **P** is oriented parallel to the beam velocity, as shown in Fig. 1, and the − sign applies when **P** is reversed. At our operating field $|\mathbf{E}|=43.63$ V/cm,

$$\mathscr{M}(\theta)=\pm|\mathbf{P}|\,3.0103\times10^{-4}\sin\theta \ . \tag{2.8}$$

The total intensity from (2.5) becomes

$$I(\theta)=\mathscr{L}(\theta)+\mathscr{M}(\theta) \ . \tag{2.9}$$

This equation is only accurate over the small angular regions near $\hat{\mathbf{k}}$ perpendicular to $\hat{\mathbf{E}}$ and near $\hat{\mathbf{k}}$ parallel to $\hat{\mathbf{E}}$, because the second small term in Eq. (2.1) has been omitted. Polar diagrams for $\mathscr{L}(\theta)$ and $\mathscr{M}(\theta)$ are shown in Fig. 2, where the anisotropy in $\mathscr{L}(\theta)$ and the relative magnitude of $\mathscr{M}(\theta)$ have been greatly exaggerated. The $He^+(2s)$ ion beam passes through the origin into the page and **P** is either parallel or antiparallel to the beam velocity **v**. The four uv photon counters *A*, *B*, *C*, and *D* view the radiation simultaneously. The radiation patterns are invariant under reversal of $\hat{\mathbf{E}}$ with the exception that $\mathscr{M}(\theta)$ reverses sign if $\hat{\mathbf{E}}$ is rotated by π radians or **P** is reversed.

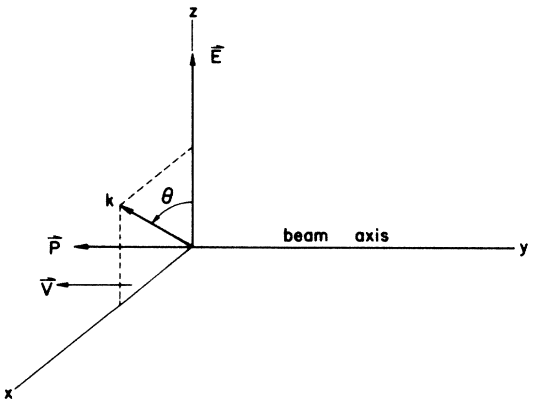

FIG. 1. Geometry of the experiment showing the electric field vector **E** in the *z* direction, the spin-polarization vector **P** in the negative *y* direction, the beam velocity vector **v**, and the direction of observation $\hat{\mathbf{k}}$ in the *xz* plane.

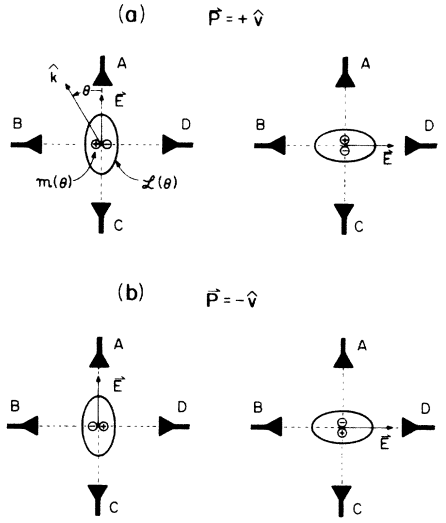

FIG. 2. Polar diagrams for two electric field directions of the quench radiation for a spin-polarized $He^+(2s)$ beam traveling through the origin into the page of the paper for (a) a spin-polarization vector **P** parallel to the beam velocity, and (b) a spin-polarization vector **P** antiparallel to the beam velocity. In arbitrary intensity units, the distributions $\mathscr{L}(\theta)=1+0.2675\cos\theta^2$ and $\mathscr{M}(\theta)=\pm|\mathbf{P}|(0.01313/|\mathbf{E}|)\times(1-0.01313/|\mathbf{E}|)^{-1}\sin\theta$ represent the main quench radiation and the *E*1-*M*1 interference term, respectively. *A*, *B*, *C*, and *D* are the uv photon detectors shown in Fig. 3.

C. The *E*1-*M*1 asymmetry

The above analysis shows that the relative intensity difference between any pair of opposite counters viewing the radiation perpendicular to the field is

$$A=\frac{I(\pi/2)-I(3\pi/2)}{I(\pi/2)+I(3\pi/2)} \ . \tag{2.10}$$

Using Eqs. (2.5), (2.2), and (2.3) and introducing the notation

$$\Delta_j = E(2s_{1/2}) - E(2p_j) + i\Gamma/2, \quad j = \tfrac{1}{2}, \tfrac{3}{2}, \tag{2.11}$$

the "left-right" asymmetry to lowest order in field strength becomes

$$A = \frac{6\,\mathrm{Re}(\Delta_{1/2})\langle 1s_{1/2,1/2} \mid M_{1,0} \mid 2s_{1/2,1/2}\rangle}{e^2 \mid \mathbf{E} \mid \langle 1s \mid z \mid 2p\rangle\langle 2p \mid z \mid 2s\rangle} \times \left[\frac{1+(\frac{1}{2}) \mid \rho \mid^2 \mathrm{Re}(\Delta_{3/2})/\mathrm{Re}(\Delta_{1/2})}{1+\mathrm{Re}(\rho)+5 \mid \rho \mid^2/2}\right], \tag{2.12}$$

where $\rho = \Delta_{1/2}/\Delta_{3/2}$. The matrix elements are

$$\langle 1s \mid z \mid 2p\rangle = 2^8/(3^5\sqrt{2}Z), \tag{2.13}$$

$$\langle 2p \mid z \mid 2s\rangle = -3/Z, \tag{2.14}$$

and

$$\langle 1s_{1/2,1/2} \mid M_{1,0} \mid 2s_{1/2,1/2}\rangle = \frac{-8\alpha^2 Z^2}{81\sqrt{2}} \frac{e\hbar}{mc}. \tag{2.15}$$

The factor in large parentheses of (2.12) is 1.026 12, and the numerical value of A is

$$A = 0.013\,13/\mid \mathbf{E}(\mathrm{V/cm}) \mid . \tag{2.16}$$

At our operating field of $\mid \mathbf{E} \mid = 43.63$ V/cm,

$$A = 3.009 \times 10^{-4}. \tag{2.17}$$

The quantity directly measured in the experiment is the intensity ratio

$$r = I(\pi/2)/I(3\pi/2) \tag{2.18}$$

in opposite directions perpendicular to the field which is related to A as

$$A = \frac{r-1}{r+1}. \tag{2.19}$$

III. EXPERIMENT

A. Overall plane

The apparatus shown in Fig. 3 is nearly identical to that in our previous experiment.[6] A 135-keV beam of spin-polarized He^+ $(2s)$ ions, after passing a prequencher and a collimator, enters into the quenching-cell proper and is monitored with a Faraday cup. The collimator limits the beam diameter to 1.5 mm. The quenching cell consists of four metal rods mounted on insulators in a quadrupole arrangement. By appropriately switching the polarities on the rods, the electric field can be rotated such that it makes an angle (see Fig. 2) of 0, $\pi/2$, π, or $3\pi/2$ with respect to any of the observation axes of the uv photon detectors.

The circular exit slits (S_2) of the photon collimators have a diameter of (1.016±0.002) cm and are mounted at a distance of (21.895±0.005) cm from the beam axis. Each of these slits is covered with a self-supporting thin film of Al (transparent to the 304-Å Lyman-α radiation) to eliminate noise counts from low-energy particles. The entrance slits (S_1) of width (1.270±0.002) cm are mounted at a distance of (7.112±0.002) cm from the beam axis.

The prequencher potentials are only switched on for noise determinations and are sufficiently strong to destroy virtually all metastable $He^+(2s)$ ions in the beam by quenching.

By using a spin polarizer, the spin-polarization vector for the electron can be set at either $\mathbf{P} = +\hat{\mathbf{v}}$ or $\mathbf{P} = -\hat{\mathbf{v}}$. The axial magnetic field inside the spin polarizer is 7 kG. With this field, the focal position falls in the center of the collimator and results in maximum beam current through the quenching cell. To ensure a sharp definition of the beam axis, a magnetic field of 10 G is applied parallel to the beam direction over the observation region. Half of this field arises from the stray magnetic field of the spin polarizer and fluctuations in it could only be kept to within 0.04 G. The other 5 G is applied with two coils located in such a manner as to cancel the field gradient of the net magnetic field along the beam direction in the observation region in first order. This eliminates the generation of rotational electric fields on the fast particles in the ion beam. A disadvantage of the magnetic field fluctuations is that they introduce small random changes in the efficiencies of the photon counters.

The ion-beam current is 6 μA and the beam consists mainly of ground-state $He^+(1s)$ ions with a metastable $He^+(2s)$ content estimated to be about 1%. The fraction of neutral particles is negligibly small since neutrals entering the spin polarizer cannot pass through the collimator

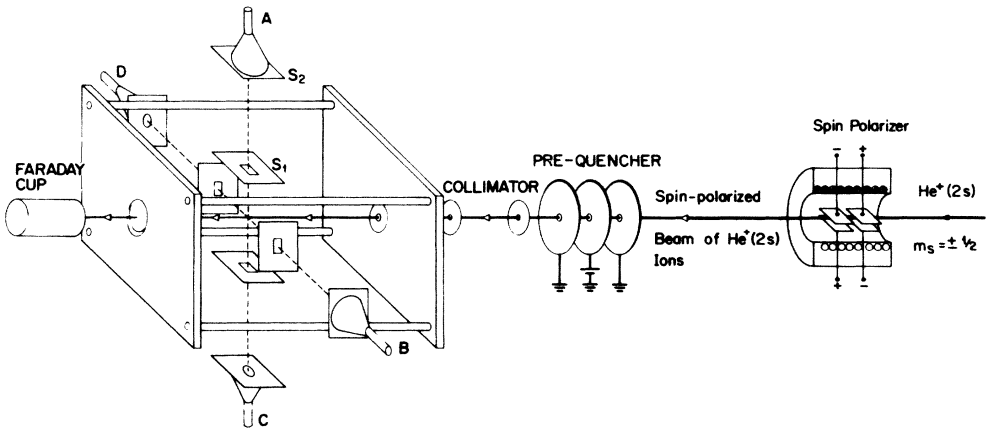

FIG. 3. Schematic diagram of the apparatus. Important dimensions are given in the text.

to enter the quenching cell.

The small signal still observed with a prequenched beam serves as a good definition for the noise level. It consists primarily of uv photons produced by excitation processes between the beam and the remaining gas in the observation region. The small signal intensity is nearly proportional to the residual gas pressure for pressures above 3×10^{-8} Torr, the best achievable vacuum. It also increases weakly with the electric field as a consequence of the formation of $He^+(2s)$ metastables by the ground-state ions in passing through the cell. The presence of metastables in the quenched beam makes the noise slightly anisotropic. The intensity along the field directions exceeds the one perpendicular to the field directions by about 4%.

B. Method of data analysis

1. The asymmetries

The left-right asymmetry defined by (2.10) can be measured with just one pair of photon counters that view the radiation in opposite directions perpendicular to **E**. The advantage of our two pairs of photon counters, namely, A and C, and B and D, is that they provide a test for the validity of our noise correction, as discussed in Sec. III B 3. They also provide a check for possible systematic effects since the two measurements for the A asymmetry with the separate counter pairs should yield identical results.

For either $\mathbf{P}=+\hat{\mathbf{v}}$ or $\mathbf{P}=-\hat{\mathbf{v}}$, the electric field is now switched through its four possible orientations and photon counts are simultaneously collected with all counters for a counting period that is the same at each field orientation. This procedure not only allows the ratio measurement r corresponding to the left-right asymmetry but also

$$R=I_{||}/I_{\perp} , \tag{3.1}$$

the ratio in the intensities emitted parallel and perpendicular to the field direction. We henceforth refer to the R asymmetry as the Lamb-shift asymmetry.

Since the A value being measured is very small ($A_{\rm th}\simeq3\times10^{-4}$), only very small fluctuations of the ion beam from its central path can be tolerated. For an experiment with a predescribed precision for A of 10%, these fluctuations for our apparatus must be limited to $\pm6\times10^{-4}$ cm. Since this condition could not be guaranteed over long periods of time, the orientation of the electric field was switched very frequently to greatly reduce the systematic errors resulting from slow beam drifts in the observation region.

We now combine the data in such a way that the relative efficiencies of the photon counters are eliminated. Let $(N_B/N_D)_\theta$ denote the intensity ratio I_B/I_D for photon counter B and D as shown in Fig. 2, where θ specifies the direction of **E** relative to its starting position as shown in the upper-left corner of the figure. For example, the two field orientations shown for $\mathbf{P}=+\hat{\mathbf{v}}$ are $\theta=0$ and $\theta=3\pi/2$. We now form the ratios

$$\begin{aligned} r_{BD}&=[(N_B/N_D)_0(N_D/N_B)_\pi]^{1/2} , \\ r_{AC}&=[(N_A/N_C)_{3\pi/2}(N_C/N_A)_{\pi/2}]^{1/2} , \end{aligned} \tag{3.2}$$

for the left-right asymmetry and the Lamb-shift ratio for the adjacent counters A and B,

$$R_{AB}=\left[\frac{(N_A)_0+(N_A)_\pi}{(N_B)_0+(N_B)_\pi}\,\frac{(N_B)_{\pi/2}+(N_B)_{3\pi/2}}{(N_A)_{\pi/2}+(N_A)_{3\pi/2}}\right]^{1/2} , \tag{3.3}$$

and similar expressions for other counter pairs. These ratios must still be corrected for noise, as described in Sec. III B 3.

2. Errors

The statistical errors in r from counting statistics alone are

$$\begin{aligned} \delta r_{BD}&=r_{BD}(1/N_B+1/N_D)^{1/2} , \\ \delta r_{AC}&=r_{AC}(1/N_A+1/N_C)^{1/2} . \end{aligned} \tag{3.4}$$

Here $N_B=(N_B)_0+(N_B)_\pi$, where $(N_B)_0$ and $(N_B)_\pi$ are measured in equal time intervals, and N_D, N_A, and N_C are similar sums. Expressions for δR are analogous to (3.4).

Since $A=(r-1)/(r+1)$ and r differs but little from unity,

$$r=1+\Delta \tag{3.5}$$

and

$$A\simeq\Delta/2 . \tag{3.6}$$

The error in A becomes

$$\delta A\simeq\tfrac{1}{2}\delta r . \tag{3.7}$$

The above equations show that $\delta A\propto1/\sqrt{N}$, where N is the total number of photon counts, which is proportional to E^2t. Hence, except for the influence of background noise, the counting time required the achieve a given relative precision in A is independent of E, since $A\propto1/E$ [see (2.12)] and $\delta A\propto1/Et^{1/2}$.

The choice of the relatively low field of $E=43.63$ V/cm represents a balance between having an adequate signal-to-noise ratio of 2:1 and not making A too small. Although the signal-to-noise ratio improves quadratically with $|\mathbf{E}|$, we deliberately kept the field very small to avoid systematic effects that conceivably might arise from excitation processes by secondary low-energy ions in the primary beam.

3. Noise correction

Since the noise counts increase weakly with the electric field, we defined the noise as the signal still observed with a prequenched beam, rather than as the signal still observed for an unquenched beam in the absence of a quenching field in the observation region. The validity of this definition is discussed in the next section. The most direct way of taking noise into account is to subtract it from the appropriate N values in (3.2). The requirements for the validity of this procedure are twofold. Firstly, the error in the noise counts must be reduced to a level comparable to that for the signal counts. In view of the low signal-to-noise ratio of about 2, the counting period for the noise then becomes 70% of that for the signal, thus

nearly doubling the total running time. Secondly, the prequenched beam must follow the same trajectory and possess the same beam profile as the unquenched beam to avoid asymmetries in the noise level that may not be present in the signal. This last condition could not be met. In fact, application of the prequenching potentials altered the ion beam, resulting in a beam-current loss as measured by the Faraday cup of as much as 1%.

Hence, we chose another way to incorporate the noise. The method follows from inspection of the A value for a single counter, for example, B in Fig. 2. It is

$$A'=\frac{N(0)-N(\pi)}{N(0)+N(\pi)} \tag{3.8}$$

where $N(0)$ and $N(\pi)$ are the "raw" measurements that include both signal and noise counts. Since the noise counts in $N(0)$ and $N(\pi)$ must be the same, only the denominator is affected by the noise. On defining the noise fraction f as

$$f=\frac{n(0)+n(\pi)}{N(0)+N(\pi)}\ , \tag{3.9}$$

where $n(0)$ and $n(\pi)$ are the noise measurements, the corrected A value is related to A' as

$$A=A'/(1-f)\ . \tag{3.10}$$

The only requirement on the f determination is that the error in $1/(1-f)$ be much less than the statistical error in A'. This condition could easily be met and the noise level was only measured once for every four signal measurements.

IV. RESULTS

In all, we obtained 2632 measurements with a spin-polarization vector $\mathbf{P}=+\hat{\mathbf{v}}$ and another 2616 measurements with $\mathbf{P}=-\hat{\mathbf{v}}$. The total photon counts after subtraction of noise perpendicular to the field and along the field directions are 1.295×10^9 and 1.637×10^9. With an ion beam of 6 μA and a quenching field $|\mathbf{E}|=43.63$ V/cm, each measurement takes 250 sec for a total counting time interval of 365 h.

A. The Lamb-shift ratio

Since the Lamb-shift ratio is well known from previous work,[7] its measured value here provides an accurate check on the noise-correction measurement. The ratios, corrected for noise and the finite solid angle of observation, are the same for each adjacent counter pair. The average values for $\mathbf{P}=\pm\hat{\mathbf{v}}$ are

$$R_+=1.2635\pm0.0001\ , \tag{4.1}$$

$$R_-=1.2654\pm0.0001\ . \tag{4.2}$$

The measured R values are slightly smaller than the expected $R=1.2675$ [see Eq. (2.6)]. In view of the large noise correction (6.5%) the discrepancy is not surprising. The noise level for a prequenched beam consisting only of $He^+(1s)$ ions, underestimates that for the unquenched beam because the overall photon-excitation cross section for $He^+(2s_{1/2})$ ions with the residual gas exceeds that for ground-state ions.

In view of the uncertainties in the noise measurement, we adopted the procedure of introducing correction factors $C_\pm$ to the noise measurements such that the measured $R_\pm$ values are brought into agreement with theory. The correction factors for $\mathbf{P}=\pm\hat{\mathbf{v}}$ are

$$C_+=1.030\ , \tag{4.3}$$

$$C_-=1.013\ . \tag{4.4}$$

The difference in C_+ and C_- can be accounted for by the slightly higher residual pressure for the former. The values are sufficiently close to unity that the corrections are small compared with other sources of error. We conclude that our definition for the noise (see Sec. III B 3) leads to noise levels with a precision of a few percent. These, in turn, can be corrected to obtain noise levels to a higher degree of precision by assuming the theoretical value for R.

B. Noise fraction for r

The observed fractions of the noise perpendicular to the electric field direction as defined by (3.9) for the various counters are nearly the same. The averages are

$$f'_+=0.340\,48\pm0.000\,04 \quad \text{for } \mathbf{P}=+\hat{\mathbf{v}}\ , \tag{4.5}$$

$$f'_-=0.327\,19\pm0.000\,04 \quad \text{for } \mathbf{P}=-\hat{\mathbf{v}}\ . \tag{4.6}$$

Correcting these by the factors of (4.3) and (4.4) yields

$$f_+=0.3507\ , \tag{4.7}$$

$$f_-=0.3313\ . \tag{4.8}$$

Their confidence level is expected to fall at least within the 1% range.

C. The left-right asymmetry

The observed ratios for opposite photon-counter pairs with polarization vector $\mathbf{P}=+\hat{\mathbf{v}}$ are

$$r_+(AC)=(1+0.000\,417\,15)\pm0.000\,085\,5\ ,$$

$$r_+(BD)=(1+0.000\,298\,35)\pm0.000\,091\,3\ ,$$

in agreement with each other, with an average of

$$\bar{r}_+=(1+0.000\,357\,75)\pm(0.000\,062\,5\pm0.000\,000\,9)\ . \tag{4.9}$$

The corresponding results for $\mathbf{P}=-\hat{\mathbf{v}}$ are

$$r_-(AC)=(1-0.000\,280\,13)\pm0.000\,087\,6\ ,$$

$$r_-(BD)=(1-0.000\,553\,03)\pm0.000\,091\,2\ .$$

Although these data points differ from each other by 1.5 error bars, discrepancies of this type occur at least once in every ten similar measurements. The average of the last two measurements is

$$\bar{r}_-=(1-0.000\,416\,58)\pm(0.000\,063\,2\pm0.000\,000\,9)\ . \tag{4.10}$$

The magnitude of the deviation from unity is in agreement with that for $\bar{r}_+$.

The experimental standard deviations in (4.9) and (4.10) are the ones from counting statistics alone. The corresponding theoretical errors are

$$\sigma_+ = 0.000\,064\,0 \pm 0.000\,001\,0 ,$$

$$\sigma_- = 0.000\,064\,7 \pm 0.000\,001\,0 ,$$

in approximate agreement with the experimental ones. That the fluctuations in our data are no worse than what can be expected from counting statistics alone, indicates that errors arising from small beam drifts in the observation cell are effectively eliminated by frequent switching of the electric field. (See Sec. III B 1.)

In Figs. 4(a) and 4(b) we compare the histograms of the experimental data distributions for $\mathbf{P} = +\hat{\mathbf{v}}$ with the theoretically expected histograms for Gaussian distributions for counter pairs A and C and B and D, respectively [see also Figs. 5(a) and 5(b)]. The χ^2 tests of the fits with the mean and the theoretical standard deviations as the only adjustable parameters yield

$$\chi^2(AC) = 34.1 ,$$

$$\chi^2(BD) = 41.5 ,$$

for 37 degrees of freedom corresponding to confidence levels of 60% and 28%, respectively. Similar results for $\mathbf{P} = -\hat{\mathbf{v}}$ are

$$\chi^2(AC) = 28.6 ,$$

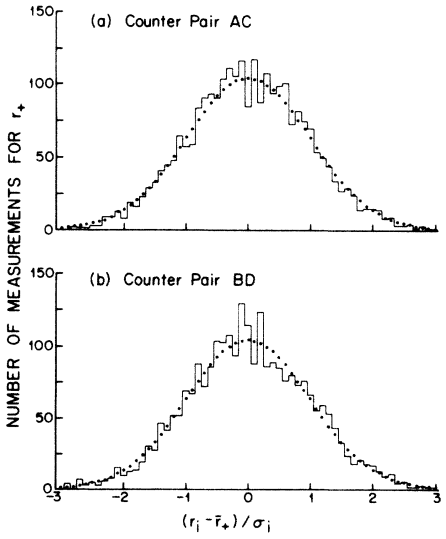

FIG. 4. Histograms for the distribution of the experimental data for r_+ about the mean in units of the theoretically expected standard deviation for each point, for (a) photon-counter pair A and C (see Fig. 3), and (b) photon-counter pair B and D. The solid points show the expected bar heights for a Gaussian distribution with the same mean and unit half-width.

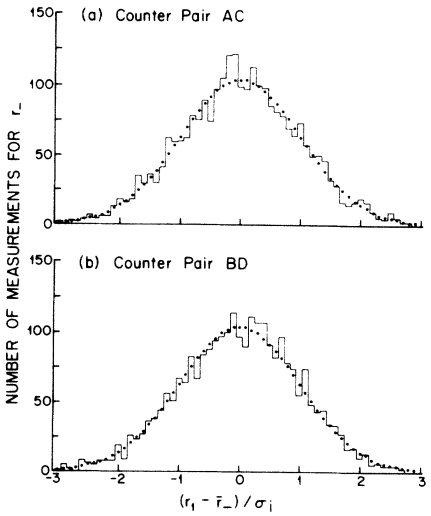

FIG. 5. Histograms for the distribution of the experimental data for r_- about the mean in units of the theoretically expected standard deviation for each point, for (a) photon-counter pair A and C (see Fig. 3), and (b) photon-counter pair B and D. The solid points show the expected bar heights for a Gaussian distribution with the same mean and unit half-width.

TABLE I. Comparison of the observed numbers of low and high runs with the expected number of runs for (a) $\mathbf{P} = +\hat{\mathbf{v}}$ and (b) $\mathbf{P} = -\hat{\mathbf{v}}$.

Run length	Low runs	High runs	Expected number
	(a)		
1	360	355	329 ±16
2	144	164	165 ±12
3	101	84	82 ± 8
4	47	41	41 ± 6
5	10	23	21 ± 4
6	11	7	10 ± 3
7	4	3	5.1 ± 2.2
8	1	2	2.6 ± 1.6
9	1	1	1.3 ± 1.1
10	2	1	0.6 ± 0.8
11	0	0	0.32± 0.56
12	0	0	0.16± 0.40
Total	681	681	658 ±13
	(b)		
1	314	314	327 ±16
2	168	176	164 ±12
3	95	91	82 ± 8
4	43	38	41 ± 6
5	15	20	20 ± 4
6	8	10	10 ± 3
7	10	3	5.1 ± 2.2
8	1	1	2.6 ± 1.6
9	1	1	1.3 ± 1.1
10	0	1	0.6 ± 0.8
11	0	0	0.32± 0.56
12	0	0	0.16± 0.40
Total	655	655	658 ±13

$$\chi^2(BD)=30.6\ ,$$

corresponding to confidence levels of 84% and 76%, respectively. None of these χ^2 tests reveal statistically significant anomalies in the data.

The results of the runs tests for the individual measurement of $r=\frac{1}{2}(r_{AC}+r_{BD})$ for $\mathbf{P}=+\hat{\mathbf{v}}$ and $\mathbf{P}=-\hat{\mathbf{v}}$ are given in Table I. These are valid statistical tests since r_{AC} and r_{BD} have been measured in sequence. The theoretical distribution is based on the assumption that the probability for a measurement to fall above the mean is the same ($\frac{1}{2}$) as the probability to fall below the mean. The agreement between the theoretical and observed distributions for $\mathbf{P}=\hat{\mathbf{v}}$ is, at best, marginal. Instabilities in beam position and small variations in the efficiences of the photon counters (see Sec. III A), may have influenced the statistics. For both $\mathbf{P}=+\hat{\mathbf{v}}$ and $\mathbf{P}=-\hat{\mathbf{v}}$, however, there are no long runs outside those predicted by statistics and we therefore conclude that there are no systematic effects in the apparatus that produced a time-dependent shift in the measurement of r during the entire counting interval of 365 h.

Substituting of (4.9) and (4.10) into (2.19) yields

$$A'_{+}=(1.789\pm0.312)\times10^{-4}\ ,$$

$$A'_{-}=(-2.083\pm0.316)\times10^{-4}\ .$$

These A' values corrected for noise, using (3.10), become

$$A_{+}=(2.755\pm0.480)\times10^{-4}\ ,$$

$$A_{-}=(-3.114\pm0.473)\times10^{-4}\ .$$

The average magnitude of A is

$$A=(2.935\pm0.337)\times10^{-4}\ , \tag{4.11}$$

in agreement with the theoretical value

$$A_{\rm th}=3.009\times10^{-4}\ \text{ for }\ |\mathbf{E}|=43.63\ \text{V/cm}\ .$$

The error in (4.11) is the one from counting statistics alone. At the 10% precision level, all other errors and corrections are negligibly small. When the experiment is regarded as a measurement of the relativistic magnetic dipole matrix element, then

$$\langle 1s_{1/2,1/2}\,|\,M_{1,0}\,|\,2s_{1/2,1/2}\rangle=-(0.2725\pm0.0313)\frac{\alpha^2e\hbar}{mc}$$

in agreement with the theoretical value of

$$-0.2794\frac{\alpha^2e\hbar}{mc}$$

obtained from (2.15).

V. CONCLUSION

We have presented an improved measurement of the magnetic dipole matrix element for the decay of the $2s_{1/2}$ state in hydrogenic He^+. Though the error is still large as a consequence of the small size of the left-right asymmetry for He^+, the precision can readily be improved by using a heavier ion since A scales as Z^5 when $|\mathbf{E}|$ is adjusted to maintain a constant quenching rate as a function of Z [see (2.12)]. The agreement obtained with theory provides a direct confirmation of the calculated relativistic corrections to the magnetic dipole transition operator at the $\pm10\%$ level of accuracy.

Although there have been no other measurements of the $2s_{1/2}$-$1s_{1/2}M1$ matrix element in hydrogenic ions, there has been considerable interest in the closely related $1s2s\ ^3S_1-1s^2\ ^1S_0M1$ transition rates of heliumlike ions from He to Kr^{34+}.[8] Some of these measurements show indications of nonexponential decay due to cascades.[9] The present experiment provides an independent check of the relativistic $M1$ transition operator which does not depend on a direct measurement of the radiative decay rate. No measurements of electric dipole ($E1$) or other decay rates in few-electron ions have been reported to date which are accurate enough to be sensitive to relativistic corrections. The present experiment therefore provides a unique opportunity to study the effects of relativity on radiative transitions.

ACKNOWLEDGMENTS

Research support by the Natural Sciences and Engineering Research Council of Canada is gratefully acknowledged.

[1]S. P. Goldman and G. W. F. Drake, Phys. Rev. A **24**, 183 (1981), and earlier references therein.

[2]F. A. Parpia and W. R. Johnson, Phys. Rev. A **26**, 1142 (1982).

[3]G. W. F. Drake, Phys. Rev. A 3, 906 (1971); G. Feinberg and J. Sucher, Phys. Rev. Lett. **26**, 681 (1971); I. L. Biegman and U. I. Safranova, Zh. Eksp. Teor. Fiz. **60**, 2045 (1971) [Sov. Phys.—JETP **33**, 1102 (1971)].

[4]H. Gould and R. Marrus, Phys. Rev. A **28**, 2001 (1983).

[5]A. van Wijngaarden and G. W. F. Drake, Phys. Rev. A **25**, 400 (1982).

[6]G. W. F. Drake, J. Patel, and A. van Wijngaarden, Phys. Rev. A **28**, 3340 (1983).

[7]G. W. F. Drake, S. P. Goldman, and A. van Wijngaarden, Phys. Rev. A **20**, 1299 (1979).

[8]For a review, see J. Sucher, in *Atomic Physics 5*, edited by R. Marrus, M. Prior, and H. Shugart (Plenum, New York, 1977), p. 415.

[9]D. L. Lin and L. Armstrong, Jr., Phys. Rev. A **16**, 791 (1977).